

## ORIGINAL ARTICLE

# Quantum spin Hall insulators and quantum valley Hall insulators of BiX/SbX (X = H, F, Cl and Br) monolayers with a record bulk band gap

Zhigang Song<sup>1,5</sup>, Cheng-Cheng Liu<sup>2,5</sup>, Jinbo Yang<sup>1,3</sup>, Jingzhi Han<sup>1</sup>, Meng Ye<sup>1</sup>, Botao Fu<sup>2</sup>, Yingchang Yang<sup>1</sup>, Qian Niu<sup>3,4</sup>, Jing Lu<sup>1,3</sup> and Yuguai Yao<sup>2</sup>

A large bulk band gap is critical for the application of quantum spin Hall (QSH) insulators or two-dimensional (2D) topological insulators (TIs) in spintronic devices operating at room temperature (RT). On the basis of first-principles calculations, we predicted a group of 2D TI BiX/SbX (X = H, F, Cl and Br) monolayers with extraordinarily large bulk gaps from 0.32 eV to a record value of 1.08 eV. These giant-gaps are entirely due to the result of the strong spin-orbit interaction related to the  $p_x$  and  $p_y$  orbitals of the Bi/Sb atoms around the two valleys  $K$  and  $K'$  of the honeycomb lattice, which is significantly different from that consisting of the  $p_z$  orbital as in graphene/silicene. The topological characteristic of BiX/SbX monolayers is confirmed by the calculated nontrivial  $Z_2$  index and an explicit construction of the low-energy effective Hamiltonian in these systems. We demonstrate that the honeycomb structures of BiX monolayers remain stable even at 600 K. Owing to these features, the giant-gap TIs BiX/SbX monolayers are an ideal platform to realize many exotic phenomena and fabricate new quantum devices operating at RT. Furthermore, biased BiX/SbX monolayers become a quantum valley Hall insulator, exhibiting valley-selective circular dichroism.

NPG Asia Materials (2014) 6, e147; doi:10.1038/am.2014.113; published online 12 December 2014

## INTRODUCTION

Quantum spin Hall (QSH) insulators, also known as two-dimensional (2D) topological insulators (TIs), have generated great interest in condensed matter physics and materials science because of their scientific importance as a novel quantum state and potential applications ranging from spintronics to topological quantum computation.<sup>1–3</sup> QSH insulators are characterized by an insulating bulk and fully spin-polarized gapless helical edge states without backscattering at the sample boundaries, which are protected by time-reversal symmetry. The prototypical concept of the QSH effect was first proposed by Kane and Mele<sup>4,5</sup> in graphene, in which the spin-orbit coupling (SOC) opens a band gap at the Dirac point. However, the rather weak second-order effective SOC makes the QSH effect in graphene only appear at an unrealistically low temperature.<sup>6</sup>

To date, only the HgTe/CdTe quantum well has been verified to be a well-established QSH insulator experimentally.<sup>7,8</sup> Experimental evidence has also been presented recently for helical edge modes in inverted InAs/GaSb quantum wells.<sup>9</sup> The critical drawback of such a reported QSH state is their small bulk gaps, which are too small to make the predicted QSH effect observable under easily accessible experimental conditions. Thus, to observe the QSH effect at room

temperature (RT) in TIs, a large bulk band gap is essential; the edge current can be stabilized against the interference of the thermally activated carriers in the bulk because the carrier concentration in the bulk decreases exponentially with the band gap. Extensive effort has been devoted to the search for new 2D TIs with a large bulk band gap.<sup>10–14</sup> Some layered materials such as silicene, germanene<sup>15</sup> and stanene<sup>16</sup> have been proposed, and the bulk band gap of 2D TI has been elevated to a remarkable 0.3 eV in a chemically modified tin film, SnX (X = F, Cl, Br and I).<sup>13</sup> Recently, ultrathin Bi films have drawn much attention as promising candidates for QSH insulators, and the 2D topological properties of the ultra-thin Bi(111) films have been reported.<sup>17</sup> To the best of our knowledge, no bulk band gap has exceeded 0.7 eV in either 2D or 3D TIs.<sup>18</sup>

Because Bi and Sb are well known for their strong SOC that can drive and stabilize the topological non-trivial electronic states, it is wise to search for large-band-gap QSH insulators based on Bi/Sb-related materials. Here, we predicted that the free-standing 2D honeycomb Bi/Sb halide and Bi/Sb hydride (we call these structures bismuthumane and stibiumane, respectively, by analogy with graphane, silicane and stanane) systems are stable huge-band-gap QSH insulators based on first-principles (FP) calculations of the structure optimization,

<sup>1</sup>State Key Laboratory for Mesoscopic Physics and School of Physics, Peking University, Beijing, China; <sup>2</sup>School of Physics, Beijing Institute of Technology, Beijing, China;

<sup>3</sup>Collaborative Innovation Center of Quantum Matter, Beijing, China and <sup>4</sup>International Center for Quantum Materials, Peking University, Beijing, China

<sup>5</sup>These authors contributed equally to this work.

Correspondence: Professor J Yang or Professor J Lu, School of Physics, Peking University, State Key Laboratory for Mesoscopic Physics and School of Physics, Peking University, Beijing 100871, China or Professor Y Yao, School of Physics, Beijing Institute of Technology, Beijing, China.

E-mail: jbyang@pku.edu.cn or jinglu@pku.edu.cn or ygao@bit.edu.cn

Received 11 February 2014; revised 25 September 2014; accepted 27 October 2014

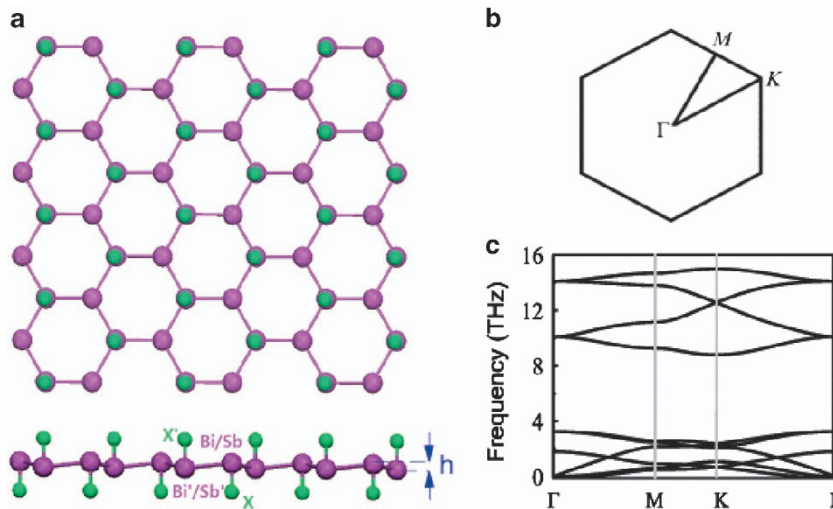


**Figure 1** (a) Lattice geometry for BiX/SbX monolayer (X=H, F, Cl and Br) from the top view (upper) and side view (lower), respectively. In a unit cell, BiX/SbX is related to Bi'X'/Sb'X' by an inversion operation. (b) The first Brillouin zone of BiX/SbX monolayers and the points of high symmetry. (c) Corresponding phonon spectrum for BiH monolayer.

**Table 1** The lattice constant  $a$ , Bi-Bi and Sb-Sb bond length  $b$ , Bi-X and Sb-X bond length  $d$ , buckling height  $h$  shown in Figure 1a ( $h$  is defined as the distance from the center of the upper to that of the lower Bi/Sb atoms), global band gap  $\Delta$  (the superscripts  $d$  and  $i$  represent the direct gap and indirect gap, respectively)

Monolayers	$a$ (Å)	$b$ (Å)	$d$ (Å)	$h$ (Å)	$\Delta$ (eV)	$v_F(10^5$ m/s)	$\lambda_{SO}$	$Z_2$
BiH	5.53	3.19	1.82	0.08	1.03 <sup>i</sup>	8.9	0.56	1
BiF	5.38	3.14	2.12	0.46	1.08 <sup>i</sup>	7.2	0.55	1
BiCl	5.49	3.17	2.54	0.24	0.95 <sup>i</sup>	6.9	0.56	1
BiBr	5.52	3.18	2.69	0.16	0.74 <sup>i</sup>	8.0	0.65	1
SbH	5.29	3.05	1.73	0.08	0.41 <sup>d</sup>	8.6	0.21	1
SbF	5.12	2.96	1.99	0.30	0.32 <sup>d</sup>	7.9	0.16	1
SbCl	5.17	2.98	2.42	0.14	0.36 <sup>d</sup>	7.7	0.18	1
SbBr	5.25	3.03	2.57	0.09	0.40 <sup>d</sup>	8.6	0.20	1

Fermi velocity  $v_F$  and magnitude of the intrinsic effective SOC  $\lambda_{SO}$  for Bi and Sb hydride/halide monolayers obtained from the first-principles calculations. Note that  $\lambda_{SO} = E_g/2$ , with the local gap  $E_g$  opened by SOC at the Dirac point.

phonon modes and finite temperature molecular dynamics (MD) as well as their electronic structures. The topological characteristic of these TIs is confirmed by the FP-calculated nontrivial  $Z_2$  index. The low-energy effective Hamiltonian (LEEH) is given to capture the low-energy long-wavelength properties of these systems. Significantly, among these new TIs, we observed a bulk band gap of approximately 1.0 eV related to the  $p_x$  and  $p_y$  orbitals of the Bi atoms in BiX (X=H, F and Cl) monolayers. To the best of our knowledge, these are the largest-band-gap TIs. Their gaps opened by SOC in the QSH phase can be effectively tuned by the X atom. All of the above features make these compounds promising for applications at RT. Moreover, when the inversion symmetry of the honeycomb lattice for BiX/SbX monolayers is broken, the BiX/SbX monolayers become a quantum valley Hall insulator, and chiral optical selectivity of the valleys is obtained.

## METHODS

For these materials, we first performed a geometry optimization including SOC interaction using the VASP package within the framework of the projector augmented wave pseudopotential method using a plane-wave basis set. The

Brillouin-zone integrations were performed on a  $9 \times 9 \times 1$   $\Gamma$ -centered  $k$  mesh. Vacuum regions with thicknesses larger than 14 Å were placed to avoid interaction between the monolayers and their periodic images. Both the atomic positions and lattice constant were relaxed until the maximal force on each relaxed atom was smaller than  $0.001 \text{ eV}\text{\AA}^{-1}$ . The cutoff energy for wavefunction expansion was set as  $1.3^* E_{\text{max}}$  of the X atoms. The stability of the optimized structure for the BiH monolayer was confirmed by a vibrational analysis using the phonopy package<sup>19</sup> with a supercell of  $5 \times 5$  unit cells. Fully relativistic band calculations were performed with the linearized augmented plane wave method implemented in the WIEN2K package, and the results are in good agreement with those generated by the VASP package. SOC was included as a second vibrational step using scalar-relativistic eigenfunctions as the basis after the initial calculation was converged to self-consistency. The relativistic  $p_{1/2}$  corrections were also considered for the  $6p$  orbital of Bi to improve the accuracy. A  $20 \times 20 \times 3$   $k$ -point grid was utilized in the first Brillouin zone sampling, and the cutoff parameter  $R_{\text{mt}} \cdot K_{\text{max}}$  was 4 for Bi(Sb)H monolayers and 6 for BiX/SbX (X=F, Cl and Br) monolayers. The Fermi energy was calculated, where each eigenvalue was temperature-broadened using a Fermi function with a broadening parameter of 0.002 Ry. The exchange-correlation functional was treated using the Perdew-Burke-Ernzerhof generalized gradient approximation throughout this study.

## RESULTS

Figure 1a plots the typical optimized geometries for BiX monolayers, which have a threefold rotational symmetry similar to that in graphene. The inversion symmetry holds for all the tested compounds. The equilibrium lattice constants, nearest neighbor Bi-X distances and buckling heights obtained through the structural optimization are listed in Table 1. A quasi-planar geometry is observed to be more stable for the BiH monolayer (bismuthumane), whereas a low-buckled configuration is more stable for the BiF, BiCl and BiBr monolayers. This finding is related to the bonding between Bi and the X atoms. Because F, Cl and Br are more electronegative than H, the bond between Bi and F atoms is stronger than that between Bi and H atoms, leading to a low buckling in BiX (X=F, Cl and Br) monolayers. The lattice constants of BiX monolayers follows the sequence of  $a(\text{F}) < a(\text{Cl}) < a(\text{Br})$ , in accordance with the electronegativity. The bond distances of the Bi-X films slightly increases with the sequence of  $d(\text{Br}) > d(\text{Cl}) > d(\text{F})$  determined by their covalent bond radii. The kinetic stability of these 2D TIs is further confirmed by the calculations of the phonon spectrum without SOC. Taking BiH

monolayer for example (Figure 1c), there is no imaginary frequency along all momenta, which indicates that this structure is kinetically stable, corresponding to an energy minimum in the potential energy surface.

The thermodynamic stability of the BiX/SbX monolayers was then verified by calculating the per-atom Gibbs free energy of formation ( $\delta G$ ),

$$\delta G = E + n_{\text{Bi}}\mu_{\text{Bi}} + n_{\text{X}}\mu_{\text{X}}, \quad (1)$$

where  $-E$  represents the cohesive energy per atom of the BiX/SbX monolayers,  $n_{\text{Bi}}$  and  $n_{\text{X}}$  are the mole fractions of Bi and X atoms, respectively, for a given structure, and  $\mu_{\text{Bi}}$  and  $\mu_{\text{X}}$  are the per-atom chemical potentials of Bi and X, respectively, at a given state. We selected  $\mu_{\text{Bi}}$  and  $\mu_{\text{X}}$  as the binding energies per atom of bulk Bi and the  $\text{X}_2$  molecule, respectively. The formation energy data of all the checked BiX/SbX monolayers are presented in Table 2. The calculated  $\delta G$  value for the BiH monolayer was 0.30 eV. Bismuthine is a chemical compound with the formula  $\text{BiH}_3$  and is stable below  $-60^\circ\text{C}$ .<sup>20,21</sup>  $\delta G$  of bismuthine is 0.53 eV.  $\delta G$  of the BiH monolayer is smaller than that of bismuthine; therefore, it is possible to synthesize a BiH monolayer. Remarkably, bismuth/antimony-halide monolayers have negative  $\delta G$ , indicating a higher thermodynamic stability relative to their elemental reservoirs.

We performed *ab initio* MD simulations using a supercell of  $3 \times 3$  unit cells at various temperatures (see Figure 2 and Supplementary Figure S1) with a time step of 1.5 fs to verify the thermal stability of the BiX monolayers. After running 1500 steps at 300 and 600 K, no bond was broken, suggesting that the structures of the BiX ( $\text{X} = \text{H}, \text{F}, \text{Cl}$  and  $\text{Br}$ ) monolayers were thermally stable even at 600 K. We also performed an *ab initio* MD simulation for a larger  $4 \times 4$  supercell for the BiH monolayer and observed that the structure of the BiH monolayer was stable after 2.25 ps at 600 K (see Supplementary Figure S2). In fact, it was observed that the Bi-X bond energy was much higher than that of the Bi-Bi bonds because of the large bond distance between Bi-Bi atoms. The snapshots of the MD simulations at higher temperature reveal that the Bi-Bi bonds are broken whereas Bi-X bonds remain at 700 K. The SbX monolayers are also stable at 300–400 K (see Supplementary Figure S1). The thermal stability of these structures enables these films to be used at or even above RT, which is very important for practical applications.

The typical band structures of the predicted systems BiH, BiF and SbF are shown in Figure 3. The band structures of other monolayers are shown in Supplementary Figure S3. The valence and conduction bands near the Fermi level are mostly composed of the  $p_x$  and  $p_y$  orbitals from the Bi atoms according to the partial band projections. Notably, the two energy bands are observed to cross linearly at the  $K$  (and  $K = -K'$ ) point, suggesting the existence of Dirac-cone-like

features in the band structure of these 2D honeycomb systems without SOC. These materials can thus be considered as a gapless semiconductor, or alternatively, as a semi-metal with zero density of states at the Fermi level. Because the honeycomb structure consists of two hexagonal Bi sublattices, the electrons in these predicted materials can formally be described by a Dirac-like Hamiltonian operator containing a two-component pseudospin operator.

When SOC is switched on, the degeneracy at the Dirac points is lifted, and the valence bands are downshifted whereas the conduction bands are upshifted, yielding a huge band gap opened by SOC for all BiX monolayers. The local gap at the Dirac point  $K$  ( $K'$ ) is a result of the first-order relativistic effect related to Bi elements. Thus, the gap is robust. In contrast, the conduction bands are downshifted, whereas the valence bands are upshifted at the  $\Gamma$  point, which produces a global indirect band gap. The X atoms mainly hybridize with the Bi atom near the  $\Gamma$  point in the conduction and valence bands. The band gap can be effectively tuned by the X atoms. The global gaps of BiX ( $\text{X} = \text{H}, \text{F}, \text{Cl}$  and  $\text{Br}$ ) monolayers range from 0.74 to 1.08 eV because of the strong SOC of the Bi atoms, especially for BiH and BiF monolayers with bulk gaps larger than 1.0 eV. For SbX ( $\text{X} = \text{H}, \text{F}, \text{Cl}$  and  $\text{Br}$ ) monolayers, the valence bands are downshifted, whereas the conduction bands are upshifted at the  $K$  point, producing a global direct band gap. The values of the gaps range from 0.3 to 0.4 eV, which are comparable with the values of the theoretically predicted chemically modified tin films.<sup>13</sup>

The band topology of BiX/SbX ( $\text{X} = \text{F}, \text{Cl}$  and  $\text{Br}$ ) monolayers can be characterized by the  $Z_2$  invariant.<sup>22</sup>  $Z_2 = 1$  characterizes a nontrivial band topology (corresponding to a QSH insulator), whereas  $Z_2 = 0$  represents a trivial band topology. The  $Z_2$  invariants can be directly obtained from the FP lattice computation method.<sup>23</sup> Taking a BiH monolayer as an example, the  $n$ -field configuration is shown in <sup>3</sup>from FP calculations. Note that different gauge choices result in different  $n$ -field configurations; however, the sum of the  $n$ -field over half of the Brillouin zone is gauge invariant module 2, namely  $Z_2$  topological invariant.<sup>24</sup> The honeycomb BiH monolayer has nontrivial band topology with the topological invariant  $Z_2 = 1$ , and at the Dirac point  $K$ , the gap opened by SOC is sizable. We also calculate the  $Z_2$  topological invariant for the other systems and find that all the invariants are topologically non-trivial. Therefore, the QSH effect can be steadily achieved in the 2D honeycomb Bi(Sb) hydride/halide with huge SOC gap.

To the best of our knowledge, a bulk band gap of greater than 1.0 eV in BiH and BiF monolayers is the largest bulk band gap of all the reported TIs. The band gaps of these compounds are approximately three times the values of the recent results of theoretically predicted chemical modified tin films (a bulk gap of 0.3 eV)<sup>13</sup> and the superstar 3D TI  $\text{Bi}_2\text{Se}_3$  (a bulk gap of 0.35 eV).<sup>25</sup> Furthermore, the predicted large bulk gap makes BiX/SbX monolayers capable of enduring considerable crystal defects and thermal fluctuation, which are beneficial to applications in high-temperature spintronics devices. Bi is among the main group elements that have the strongest SOC, a fundamental mechanism to induce the  $Z_2$  topology. Therefore, the predicted TIs consisting of Bi exhibit huge gaps opened by SOC.

The bulk band gap is one of the most important parameters for TIs and is analogous to the superconducting transition temperature ( $T_c$ ) for a superconductor. Insulation of the bulk is critical to observe the surface metallic state of a TI because the surface metallic state would be masked if the bulk state becomes metallic. A large bulk band gap is critical to maintain bulk insulating. If the bulk band gap is too small, the defect and disorder, which are difficult to avoid in material growth,

**Table 2** Comparisons between Gibbs free energies of BiX/SbX monolayers and those of  $\text{BiX}_3/\text{SbX}_3$  molecules

Monolayer	$\delta G$ (eV)	Molecule	$\delta G$ (eV)
BiH	0.299	$\text{BiH}_3$	0.53
BiF	-1.23	$\text{BiF}_3$	-1.976
BiCl	-0.509	$\text{BiCl}_3$	-0.792
BiBr	-0.412	$\text{BiBr}_3$	-0.899
SbH	0.219	$\text{SbH}_3$	0.264
SbF	-1.288	$\text{SbF}_3$	-2.204
SbCl	-0.478	$\text{SbCl}_3$	-0.858
SbBr	-0.374	$\text{SbBr}_3$	-0.579

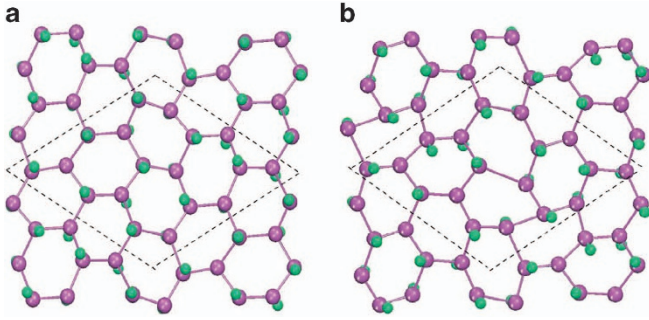


**Figure 2** Snapshots from the MD simulation of the structure for BiH monolayer at 300 K (a) and 600 K (b) after 2.25 ps. Pink balls: Bi atoms; green balls: H atoms; the dashed line indicates a supercell with a  $3 \times 3$  unit cell.

would most likely shift the Fermi level to the conduction or valence band, making the bulk conductive. In addition, if the bulk band gap is too small, carriers (electrons and holes) can be more easily produced at a finite temperature. The generations of the TIs can be categorized chiefly in terms of their bulk band gap values:<sup>1,26</sup> The first-generation TIs include Bi-Sb alloy with a bulk gap smaller than 0.1 eV, and the second-generation TIs include  $\text{Bi}_2\text{Se}_3$ ,  $\text{Sb}_2\text{Te}_3$  and  $\text{Bi}_2\text{S}_3$ . The previously reported TIs  $\text{SnX}$  ( $X = \text{F}, \text{Cl}, \text{Br}$  and  $\text{I}$ ) can also be categorized into this generation. Our reported TI BiX ( $X = \text{H}, \text{F}, \text{Cl}$  and  $\text{Br}$ ) monolayers have a bulk band gap of approximately 1.0 eV and can be regarded as third-generation TIs. Therefore, although the idea to realize a new TI by functionalization of a 2D material in this study is similar to that in our previous work, our results predict a new generation of TIs and represent an important breakthrough in the study of TIs.

Large lattice distortion greatly affects the energy band and band gap of a BiH monolayer. On the basis of MD calculations, we predicted that the phase transition temperature of the BiH monolayer is between 600 and 700 K. At 600 K, the lattice distortion is very large, and the inversion symmetry is destroyed (see Figure 2). However, the band gap remains larger than 0.22 eV after 2.25 ps. The bands are split by SOC in the absence of inversion symmetry, and the splitting is mainly a Rashba type. We calculated the  $Z_2$  number of the structure of the MD simulation at 600 K after 2.25 ps and observed that the BiH monolayer remains a TI. Hence, the topology of the BiH monolayer is very robust against a lattice distortion.

We also studied the effects of inversion symmetry breaking induced by an electric field on the band gap and topology of a BiH monolayer. The band gap was observed to decrease with increasing electric field (see Supplementary Figure S4) and closes at  $E = 0.67 \text{ V/\AA}$ ; however, the nontrivial topology remains. It is noteworthy that under a certain range of electric fields (0.61–0.67 V/\AA), BiX monolayers may generate perfect free electron gas and serve as a spin field effect transistor (see details in the Supplementary Information).

The nontrivial topology of  $\text{SnX}$  monolayers in the previous work originates from  $s$ - and  $p$ -band inversion at the  $\Gamma$  point similar to that in a HgTe quantum well and in  $\text{Bi}_2\text{Se}_3$ .<sup>8,25</sup> However, the nontrivial topology in BiX/SbX monolayers results from the massive Dirac cone, and there is no band inversion. In fact, the origin of the nontrivial topology in BiX/SbX monolayers is similar to that in graphene and silicene; however, the type of SOC in BiX/SbX monolayers is brand new. We constructed a minimal model Hamiltonian based on FP calculations and general symmetry considerations. The symmetry of these systems possesses a  $D_{3d}$  point group, and the groups of the wave vector at the Dirac points  $K$  and  $K'$  are both  $D_3$ , which splits the

$p$  orbitals at the Dirac points into two groups:  $A_2$  ( $p_z$ ) and  $E$  ( $p_x, p_y$ ). On the basis of the FP calculations, around the Dirac points and Fermi level, the low-energy band structure mainly consists of  $p_x$  and  $p_y$  orbitals from Bi/Sb atoms in the band components. The  $p_x$  and  $p_y$  orbitals form a 2D irreducible representation of the wave vector of  $D_3$  at the Dirac points, which is relevant for the low-energy physics. There are massive Dirac cones at the  $K(K')$  point and flat bands (the second band below the Fermi level)<sup>27</sup> in BiX/SbX monolayers. Massive Dirac cones and flat bands mainly consisting of the  $p_x$  and  $p_y$  orbitals distinguish BiX/SbX monolayers from graphene/silicene and lead to new phenomena, such as the orbital analog of the quantum anomalous Hall effect<sup>28</sup> and Wigner crystallization.<sup>27</sup>

Considering that there are two distinct sites, A and B, in the unit cell (Figure 1a), the symmetry-adopted basis functions can be written as  $|\Phi_1\rangle = -\frac{1}{\sqrt{2}}(p_x^A + i\tau_z p_y^A)$ ,  $|\Phi_2\rangle = \frac{1}{\sqrt{2}}(p_x^B - i\tau_z p_y^B)$ , with  $\tau_z$  representing the valley degree of freedom,  $K$  and  $K'$ , which indicates that the basis functions are different around the  $K$  and  $K'$  points. The SOC term generally reads  $H_{\text{SO}} = \xi_0 \vec{L} \cdot \vec{S} = \xi_0 \left( \frac{L_+ S_- + L_- S_+}{2} + L_z S_z \right)$ , where  $S_{\pm} = S_x \pm iS_y$  and  $L_{\pm} = L_x \pm iL_y$  denote the creation (annihilation) operator for the spin and angular momentum, respectively.  $\xi_0$  is the magnitude of effective intrinsic SOC. A straightforward calculation leads to the on-site SOC in the spinful low-energy Hilbert subspace  $\left\{ \left| \Phi_1^\uparrow \right\rangle, \left| \Phi_1^\downarrow \right\rangle, \left| \Phi_2^\uparrow \right\rangle, \left| \Phi_2^\downarrow \right\rangle \right\}$ ,  $H_{\text{SO}} = S_z \lambda_{\text{SO}} \tau_z \sigma_z$ , with  $\lambda_{\text{SO}} = \frac{1}{2} \xi_0$ . The low-energy Hilbert subspace consisting of  $p_x$  and  $p_y$  orbitals differs significantly from that consisting of a  $p_z$  orbital similar to in graphene and silicene. Moreover, the SOC term is on-site rather than the next nearest neighbor as in the Kane-Mele model.<sup>4,5,15,16</sup> This finding indicates that the SOC mechanism in BiX/SbX monolayers is completely different from that in graphene or silicene.

To the first order of  $k$ , the symmetry-allowed four-band LEEH involving SOC can be written as

$$H = \hbar v_F (k_x \sigma_x + \tau k_y \sigma_y) + S_z \lambda_{\text{SO}} \tau_z \sigma_z, \quad (2)$$

where the Pauli matrix  $\sigma$  denotes  $|\Phi_1\rangle$  and  $|\Phi_2\rangle$  orbital degrees of freedom, and  $\tau_z$  represents the valley degree of freedom  $K$  and  $K'$ . The energy spectrum of the total LEEH is  $E(\vec{k}) = \pm \sqrt{\hbar^2 v_F^2 k^2 + \lambda_{\text{SO}}^2}$  with a gap  $E_g = 2\lambda_{\text{SO}}$  at the Dirac points. The above LEEH is invariable under the space reversal and the time reversal operation. In fact, the low-energy basis functions are mixed with small components of other orbitals (see Figure 3), whereas the low-energy physics can be grasped by the low-energy effective model. The only two parameters  $v_F$  and  $\lambda_{\text{SO}}$  in the above effective Hamiltonian can be obtained from FP calculations, whose values are listed in Table 1. The band structures around the  $K$  point for BiH, BiF and SbF monolayers calculated using the DFT and LEEH methods are compared in Figure 4. It is apparent that in the vicinity of the Dirac  $K$  point, there is good agreement between the calculated results of these two methods.

There is a valley degree of freedom in BiX/SbX monolayers, and the SOC opens a large gap at the corners of the Brillouin zone. If the inversion symmetry is broken in BiX/SbX monolayers, for example by a vertical electric field, the valley-contrast Berry curvature appears, and the monolayers become a quantum valley Hall insulator. In contrast,  $\text{SnX}$  monolayers are not a quantum valley Hall insulator at all (the band gap appears at the  $\Gamma$  point).<sup>13</sup> The valley-contrast Berry curvature and spin in BiX/SbX monolayers will yield novel transport properties, such as the valley Hall effect,<sup>29</sup> valley spin Hall effect<sup>30</sup> and valley orbital moment Hall effect. In addition, valley-contrast circular dichroism will appear. Generally, the degree of valley polarization  $\eta(\mathbf{k})$  and circular dichroism can be described by the degree of circular

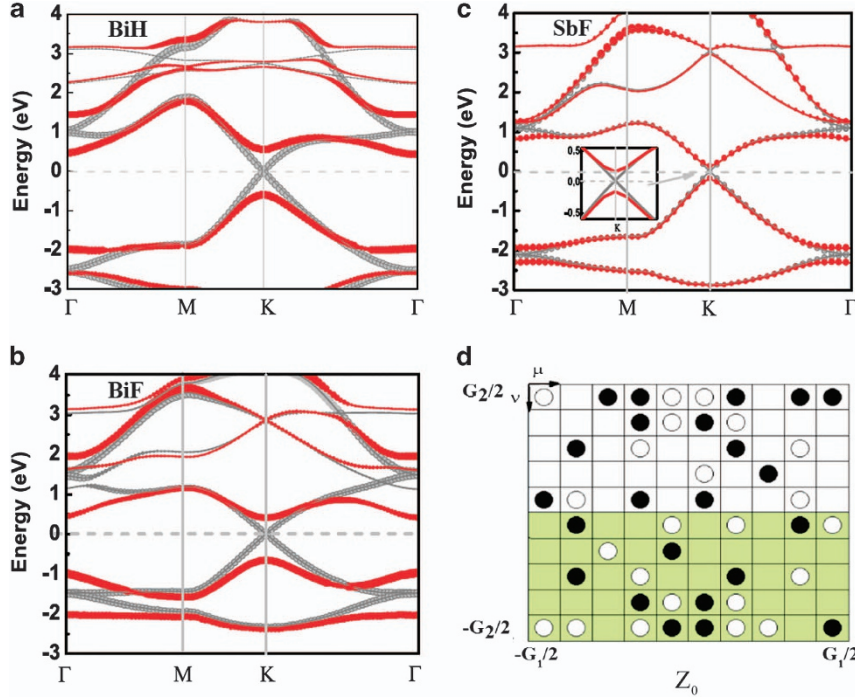


**Figure 3** Band structures of the BiX monolayers without (gray) and with (red) the SOC and  $Z_2$  topological invariant: (a) BiH, (b) BiF and (c) SbF monolayers. The Fermi level is set to zero. The bands near the Fermi level consist of the  $p_x$  and  $p_y$  orbitals. The size of the symbols is proportional to the population of the  $p_x$  and  $p_y$  orbitals. (d)  $n$ -field configuration for BiH monolayer. The calculated torus in the Brillouin zone is spanned by  $G_1$  and  $G_2$ . Note that the two reciprocal lattice vectors form an angle of  $120^\circ$ . The white and black circles represent  $n=1$  and  $-1$ , respectively, while the blank represents 0. The  $Z_2$  invariant is 1, obtained by summing the  $n$ -field over half of the torus mod 2.

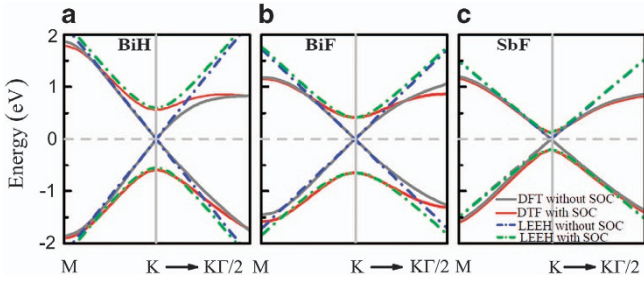


**Figure 4** A comparison of the band structures near the  $K$  point for (a) BiH, (b) BiF and (c) SbF monolayers calculated using DFT and LEEH methods. The solid gray and solid red lines denote the data calculated using DFT theory without SOC and with SOC, respectively. The dashed blue and dashed green lines represent the data calculated using the LEEH method with SOC and without SOC, respectively. The Fermi level is set to zero.

polarization  $\eta(\mathbf{k})$  in the Brillouin zone.  $\eta(\mathbf{k})$  is defined as  $\eta(\mathbf{k}) = \frac{|p_+(k)|^2 - |p_-(k)|^2}{|p_+(k)|^2 + |p_-(k)|^2}$ , where  $P_\pm = P_x \pm iP_y$  and  $p_\alpha$  is the matrix element between the conduction and valence bands and is given by  $P_x = \langle u_v(\mathbf{k}) | \frac{1}{\hbar} \frac{\partial H}{\partial k_x} | u_c(\mathbf{k}) \rangle$ .  $|u_c(\mathbf{k})\rangle$  and  $|u_v(\mathbf{k})\rangle$  are the periodic parts of the conduction and valence band of the Bloch function, respectively. The calculated  $\eta(\mathbf{k})$  in the irreducible Brillouin zone of the BiH monolayer under a vertical field is shown in Figure 5, and a perfect optical selection rule at two valleys is apparent. Namely, the valley  $K$  absorbs left-handed photons, whereas the valley  $K'$  absorbs right-handed photons. Thus, a circular polarized light can be used to create imbalanced electron occupation between the two valleys in BiX/SbX monolayers. However, in graphene and silicene, valleytronics is difficult to achieve because of the quite small SOC.

Moreover, in BiX/SbX monolayers, there is a new and strong coupling between spin and valley pseudo-spin because of the large band gap opened by SOC, which is different from that in the  $\text{MoS}_2$  system. The valley pseudo-spin can be controlled using the electric field due to the strong spin-orbital coupling in the BiX/SbX monolayers. According to the low-power model, there is an intrinsic valley degree of freedom, and the valley orbital moment couples to the spin. The low-energy effective model with broken inversion symmetry in BiX/SbX monolayers is

$$H = \hbar v_F (k_x \sigma_x + \tau k_y \sigma_y) + S_z \lambda_{SO} \tau_z \sigma_z + \frac{\Delta_1}{2} \sigma_z, \quad (3)$$

where  $\Delta_1$  is the additional band gap induced by inversion symmetry breaking. In the low-energy limit, the valley magnetic moments of BiX/SbX systems can be expressed as  $m = \tau_z s_z \frac{e \hbar v_F^2}{2 \lambda_{SO} + \Delta_1}$ , where  $s_z$  is the real spin. In contrast, in the  $\text{MoS}_2$  monolayer, the valley moments are<sup>31</sup>  $m = \tau_z \frac{e \hbar v_F^2}{2 \lambda_{SO}}$ . The valley magnetic moments of BiX/SbX monolayers are related to not only the valley pseudo-spin but also the real spin.  $\Delta_1$  is a variable that can be adjusted by the electric field.

## DISCUSSION

Chemical functionalization of 2D materials is a powerful tool to create new materials with desirable features, such as graphene or fluorinated graphene. In the current study, we have investigated the properties of a bismuth monolayer with planar or low-buckled structure and observed that its structure is unstable without the X atom. The high-buckled Bi monolayer, that is, bilayer bismuth film with a lattice constant of  $4.52 \text{ \AA}$ , is more stable than the bismuth planar monolayer with a lattice constant of approximately  $5.4 \text{ \AA}$ .<sup>11</sup> High-buckled bismuth monolayers compounded with X elements may increase their crystal lattice constants by approximately  $1.0 \text{ \AA}$ , resulting in a quasi-

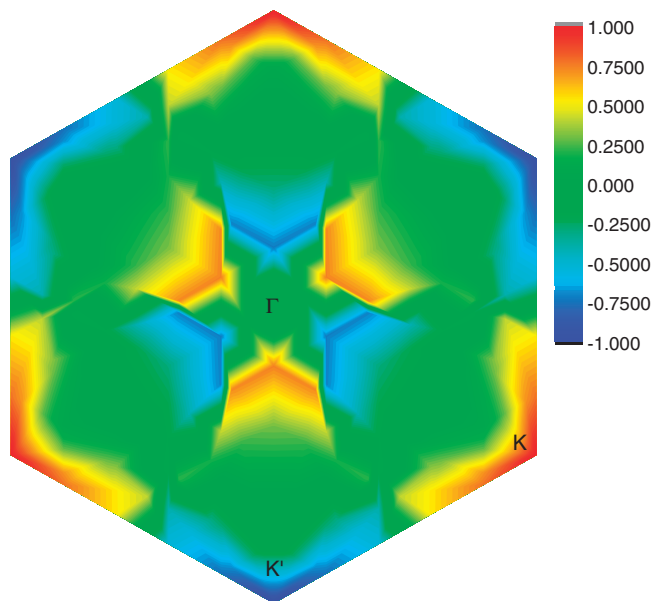


**Figure 5** Degree of circular polarization  $\eta(\mathbf{k})$  in irreducible Brillouin zone of BiH monolayer under a vertical electric field.

planar or low-buckled monolayer configuration. BiX monolayers exhibit completely different band structures from bismuth monolayers characterized by a doubled bulk band gap. In fact, we observed that the chemical functionalization of As, P and N monolayers can also result in 2D TIs with bulk band gaps of 0.18, 0.03 and 0.01 eV, respectively. Therefore, functionalization is an effective approach to obtain 2D TIs. On the experimental side, it has been known that stable halides of Bi and Sb such as BiX/SbX ( $X = \text{F, Cl, Br}$  and  $\text{I}$ )<sup>32,33</sup> have been synthesized, although hydrides of Bi and Sb are unstable at RT.<sup>20,21</sup>

Four different preparation methods were proposed here: (i) The method to synthesize graphane<sup>34</sup> may be applied to prepare BiH monolayers. High-buckled monolayer bismuth can be prepared by peeling off the bulk bismuth.<sup>17</sup> A bismuth monolayer should first be annealed in an argon atmosphere to remove any possible contamination and then exposed to cold hydrogen plasma.<sup>34</sup> (ii) Before hydrogenation, monolayer bismuth samples are heated in vacuum to remove physisorbed polymers and other contaminants that might block the hydrogenation of the graphene surface. Monolayer bismuth can be exposed to hydrogen gas under suitable conditions. Hydrogenation can be performed in a vacuum system equipped with a hot tungsten filament that can split the  $\text{H}_2$  gas into hydrogen atoms.<sup>35,36</sup> (iii) Monolayer bismuth samples are deposited on Si wafers. Then, a layer of hydrogen silsesquioxane is coated on the bismuth samples, and the samples are irradiated with electrons at various doses.<sup>37</sup> Hydrogen atoms are generated *in situ* by breaking the Si-H bonds of hydrogen silsesquioxane during the e-beam lithography process. Finally, a BiH monolayer is formed. (iv) According to the exfoliation mechanism of monolayer BN using molten hydroxides,<sup>38</sup> the bulk bismuth might be exposed to a cold hydrogen plasma to grow the BiH monolayer. When Bi atoms on the surface of bulk bismuth are combined with hydrogen atoms, the Bi-Bi bonding becomes longer, and the bismuth layer with hydrogen can be separated from the bulk. After a certain time, a BiH monolayer might form. Upon acceptance of our paper, we notice that Zhou *et al.*<sup>39</sup> just published a paper proposing to grow large-gap QSH insulator on semiconductor surface.

The MD simulation indicates that BiX monolayers will deform to some degree if the partial concentration of oxygen gas is high at RT; however, their honeycomb structure can remain (see details in the Supplementary Information (II)). BiX monolayers should be protected under vacuum or using an inert gas environment or an anti-oxidation layer such as 2D graphene, BN or  $\text{MoS}_2$ . The application of strain can further modify the band gaps of the BiX/SbX monolayers. For example, a strain of 5% can increase the band gap of a BiH monolayer by 0.06 eV (see Supplementary Figure S5).

In conclusion, we have identified a new family of huge-gap 2D TI phase BiX/SbX monolayers ( $X = \text{H, F, Cl}$  and  $\text{Br}$ ) using FP calculations, especially BiH and BiF monolayers with known largest bulk band gaps ( $> 1.0$  eV) that far exceed the gaps of the current experimentally realized 2D TI materials. The topological characteristic of these TIs are confirmed by the calculated nontrivial  $Z_2$  index and an explicit construction of the low-energy effective model in the system. These giant-gaps are entirely due to the result of strong spin-orbit interaction being related to the  $p_x$  and  $p_y$  orbitals of the Bi/Sb atoms around the two valley  $K$  and  $K'$  of the honeycomb lattice, which is sufficiently large for practical application at RT. The newly discovered BiX monolayer structure survives even at a 600 K. These results represent a significant advance in the study of TIs are expected to stimulate further work to synthesize, characterize and utilize these new 2D TIs for fundamental exploration and practical applications at RT. In addition, the biased BiX/SbX monolayers become a quantum valley Hall insulator, and valley-selective circular dichroism is available. We observe a strong coupling between the real spin and the valley pseudo-spin, which is induced by the large SOC and modified the valley magnetic moments.

## CONFLICT OF INTEREST

The authors declare no conflict of interest.

## ACKNOWLEDGEMENTS

This work was supported by the MOST Project of China (Nos. 2010CB833104, 2014CB920903, 2011CBA00100 and 2013CB932604), the National Natural Science Foundation of China (Nos. 51371009, 51171001, 11174337, 11225418, 50971003 and 11274016), the National High Technology Research and Development Program of China (No. 2011AA03A403), the Specialized Research Fund for the Doctoral Program of Higher Education of China (Nos. 20121101110046 and 20130001110002) and the Excellent Young Scholars Research Fund of the Beijing Institute of Technology (No. 2013YR1816).

*Author contributions:* Z.S., J.Y., J.L. and Y.Y. conceived the research. Z.S., B.F. and M.Y. performed the calculations. C.-L. and Z.S. performed the analysis. Z.S., C.-L., J.Y., J.L. and Y.Y. wrote the manuscript. J.H., Y.Y., Q.N., J.L. and Y.Y. contributed to the discussions and editing of the manuscript.

- Hasan, M. Z. & Kane, C. L. Colloquium: topological insulators. *Rev. Mod. Phys.* **82**, 3045 (2010).
- Qi, X.-L. & Zhang, S.-C. Topological insulators and superconductors. *Rev. Mod. Phys.* **83**, 1057 (2011).
- Yan, B. & Zhang, S.-C. Topological materials. *Rep. Prog. Phys.* **75**, 096501 (2012).
- Kane, C. L. & Mele, E. J. Quantum spin Hall effect in graphene. *Phys. Rev. Lett.* **95**, 226801 (2005).
- Kane, C. L. & Mele, E. J.  $Z_2$  topological order and the quantum spin Hall effect. *Phys. Rev. Lett.* **95**, 146802 (2005).
- Yao, Y. G., Ye, F., Qi, X. L., Zhang, S. C. & Fang, Z. Spin-orbit gap of graphene: First-principles calculations. *Phys. Rev. B* **75**, 041401(R) (2007).
- Bernevig, B. A., Hughes, T. L. & Zhang, S. C. Quantum spin Hall effect and topological phase transition in HgTe quantum wells. *Science* **314**, 1757–1761 (2006).
- König, M., Wiedmann, S., Brüne, C., Roth, A., Buhmann, H., Molenkamp, L. W., Qi, X. L. & Zhang, S. C. Quantum spin Hall insulator state in HgTe quantum wells. *Science* **318**, 1148047 (2007).

- 9 Knez, I., Du, R. R. & Sullivan, G. Andreev reflection of helical edge modes in InAs/GaSb quantum spin Hall insulator. *Phys. Rev. Lett.* **109**, 186603 (2012).
- 10 Murakami, S. Quantum spin Hall effect and enhanced magnetic response by spin-orbit coupling. *Phys. Rev. Lett.* **97**, 236805 (2006).
- 11 Liu, Z., Liu, C. X., Wu, Y. S., Duan, W. H., Liu, F. & Wu, J. Stable nontrivial  $Z_2$  topology in ultrathin Bi(111) films: a first-principles study. *Phys. Rev. Lett.* **107**, 136805 (2011).
- 12 Weeks, C., Hu, J., Alicea, J., Franz, M. & Wu, R. Q. Engineering a robust quantum spin Hall state in graphene via adatom deposition (vol X1, 021001, 2011). *Physical Review X* **2**, 029901 (2012).
- 13 Xu, Y., Yan, B., Zhang, H. J., Wang, J., Xu, G., Tang, P., Duan, W. & Zhang, S. C. Large-gap quantum spin Hall insulators in tin films. *Phys. Rev. Lett.* **111**, 136804 (2013).
- 14 Wang, Z. F., Liu, Z. & Liu, F. Organic topological insulators in organometallic lattices. *Nat. Commun* **4**, 2451 (2013).
- 15 Liu, C. C., Feng, W. X. & Yao, Y. G. Quantum spin Hall effect in silicene and two-dimensional germanium. *Phys. Rev. Lett.* **107**, 076802 (2011).
- 16 Liu, C. C., Jiang, H. & Yao, Y. G. Low-energy effective Hamiltonian involving spin-orbit coupling in silicene and two-dimensional germanium and tin. *Phys. Rev. B* **84**, 195430 (2011).
- 17 Yang, F., Miao, L., Wang, Z. F., Yao, M. Y., Zhu, F., Song, Y. R., Wang, M. X., Xu, J. P., Fedorov, A. V., Sun, Z., Zhang, G. B., Liu, C., Liu, F., Qian, D., Gao, C. L. & Jia, J. F. Spatial and energy distribution of topological edge states in single Bi(111) bilayer. *Phys. Rev. Lett.* **109**, 016801 (2012).
- 18 Yan, B. H., Jansen, M. & Feiser, C. A large-energy-gap oxide topological insulator based on the superconductor BaBiO<sub>3</sub>. *Nat. Phys.* **9**, 709–711 (2013).
- 19 Togo, A., Oba, F. & Tanaka, I. First-principles calculations of the ferroelastic transition between rutile-type and CaCl<sub>2</sub>-type SiO<sub>2</sub> at high pressures. *Phys. Rev. B* **78**, 134106 (2008).
- 20 Gillespie, R. J. & Passmore, J. *Advances in inorganic chemistry & radiochemistry* (eds Emeleus H. J., Sharp A. G.) pp 77–78 (Academic Press, 1975) ISBN 0-12-023617-6.
- 21 Greenwood, N. N. & Earnshaw, A. *Chemistry of the elements*, 2nd Edn. (Butterworth-Heinemann: Oxford, 1997) ISBN 0-7506-3365-4.
- 22 Fu, L. & Kane, C. L. Time reversal polarization and a  $Z_2$  adiabatic spin pump. *Phys. Rev. B* **74**, 195312 (2006).
- 23 Feng, W. X., Wen, J., Zhou, J. J., Xiao, D. & Yao, Y. G. First-principles calculation of  $Z_2$  topological invariants within the FP-LAPW formalism. *Comput. Phys. Commun.* **183**, 1849–1859 (2012).
- 24 Fukui, T. & Hatsugai, Y. Quantum spin Hall effect in three dimensional materials: Lattice computation of  $Z_2$  topological invariants and its application to Bi and Sb. *J. Phys. Soc. Jpn* **76**, 053702 (2007).
- 25 Zhang, H. J., Dang, W., Cha, J. J., Li, H., Meister, S., Peng, H., Liu, Z. & Cui, Y. Topological insulators in Bi<sub>2</sub>Se<sub>3</sub>, Bi<sub>2</sub>Te<sub>3</sub> and Sb<sub>2</sub>Te<sub>3</sub> with a single Dirac cone on the surface. *Nat. Phys.* **5**, 438–442 (2009).
- 26 Moore, J. Topological insulators: The next generation. *Nat. Phys.* **5**, 378–380 (2009).
- 27 Wu, C. J., Bergman, D., Balents, L. & Sarma, S. D. Flat bands and Wigner crystallization in the Honeycomb optical lattice. *Phys. Rev. Lett.* **99**, 070401 (2007).
- 28 Wu, C. J. Orbital analog of the quantum anomalous Hall effect in p-band systems. *Phys. Rev. Lett.* **101**, 186807 (2008).
- 29 Xiao, D., Yao, W. & Niu, Q. Valley-contrasting physics in graphene: magnetic moment and topological transport. *Phys. Rev. Lett.* **99**, 236809 (2007).
- 30 Xiao, D., Liu, G.-B., Feng, W., Xu, X. & Yao, W. Coupled spin and valley physics in monolayers of MoS<sub>2</sub> and other group-VI dichalcogenides. *Phys. Rev. Lett.* **108**, 196802 (2012).
- 31 Xu, X., Yao, W., Xiao, D. & Heinz, T. F. Spin and pseudospins in layered transition metal dichalcogenides. *Nat. Phys.* **10**, 343–350 (2014).
- 32 Godfrey S.M., McAuliffe C.A., Mackie A.G., Pritchard R.G., Nicholas C.N. (ed.) *Chemistry of arsenic, antimony, & bismuth*, pp 67–84 (Springer, 1998) ISBN 0-7514-0389-X.
- 33 Wiberg, E., Wiberg, N. & Holleman, A. F. *Inorganic chemistry*, Academic Press (2001) ISBN 0-12-352651-5.
- 34 Elias, D., Nair, R. R., Mohiuddin, T. M., Morozov, S. V., Blake, P., Halsall, M. P., Ferrari, A. C., Boukhalov, D. W., Katsnelson, M. I., Geim, A. K. & Novoselov, K. S. Control of graphene's properties by reversible hydrogenation: evidence for graphene. *Science* **323**, 610–613 (2009).
- 35 Sun, Z., Pint, C. L., Marcano, D. C., Zhang, C., Yao, J., Ruan, G., Yan, Z., Zhu, Y., Hauge, R. H. & Tour, J. M. Towards hybrid superlattices in graphene. *Nat. Commun.* **2**, 559 (2011).
- 36 Balog, R., Jørgensen, B., Nilsson, L., Andersen, M., Rienks, E., Bianchi, M., Fanetti, M., Laegsgaard, E., Baraldi, A., Lizzit, S., Sijivancanin, Z., Besenbacher, F., Hammer, B., Pedersen, T. G., Hofmann, P. & Hornekaer, L. Bandgap opening in graphene induced by patterned hydrogen adsorption. *Nat. Mater.* **9**, 315–319 (2010).
- 37 Ryu, S., Han, M. Y., Maultzsch, J., Heinz, T. F., Kim, P., Steigerwald, M. L. & Brus, L. E. Reversible basal plane hydrogenation of graphene. *Nano Lett.* **8**, 4597–4602 (2008).
- 38 Pakdel, A., Bando, Y. & Golberg, D. Nano boron nitride flatland. *Chem. Soc. Rev.* **43**, 934–959 (2014).
- 39 Zhou, M., Ming, W., Liu, Z., Wang, Z., Li, P. & Liu, F. Epitaxial growth of large-gap quantum spin Hall insulator on semiconductor surface. *PNAS* **111**, 14378–14381 (2014).



This work is licensed under a Creative Commons Attribution-NonCommercial-ShareAlike 4.0 International License. The images or other third party material in this article are included in the article's Creative Commons license, unless indicated otherwise in the credit line; if the material is not included under the Creative Commons license, users will need to obtain permission from the license holder to reproduce the material. To view a copy of this license, visit <http://creativecommons.org/licenses/by-nc-sa/4.0/>

Supplementary Information accompanies the paper on the NPG Asia Materials website (<http://www.nature.com/am>)